7

Wireless Communications and Power Supply for *In Vivo* Biomedical Devices using Acoustic Transmissions

Graham Wild and Steven Hinckley
Edith Cowan University
Australia

1. Introduction

Acoustic transmissions are investigated for use in the wireless transmission of digital communications signals and power supply for *in vivo* biomedical devices. The acoustic transmissions are intended to be used for fixed implanted biomedical devices, such as pacemakers, but more importantly, neural implants were wired and wireless radio frequency communications cannot be used. The acoustic transmissions can be used for both wireless communications and to recharge the device, *in vivo*, using conventional piezoelectric power harvesting techniques.

Current research in biomedical engineering is looking at implantable devices to regulate conditions such as Parkinson's and other neuromuscular conditions (Varadan, 2007). Transient devices, such as those used in the gastrointestinal track, make use of high frequency RF, were the permittivity of the human body begins to decrease (Kim et al., 2007). However, significant power is still required. This results in local tissue heating, due to the absorption of the electromagnetic radiation. This heating has side effects that limit the exposure times for safe practices (Gabriel, 1996a; b; c). For neural implants, were the goal is to have the product implanted for long periods of time, without complications and minimal side effects, radio frequency communications cannot currently be used. Acoustic transmissions represent an ideal low power method of communicating with *in vivo* biomedical devices, and for recharging them through the use of piezoelectric based power harvesting. Acoustic transmissions have previously been demonstrated as a means of communicating through elastic solids, with applications to NDT and structural health monitoring (Wild & Hinckley, 2010).

In this work, results presented show the general performance of the acoustic communications channel and sample digital communications signals, through a biological specimen, *in vivo*. The frequency response, transfer function, and transient response (at resonance) of the communications channel were measured. Due to the frequency response of the communications channel, phase shift keying has the best signal performance. To show this, the three basic digital encoding methods were tested. Successful communication was achieved through the communications channel using all three methods. The results support the hypothesis that phase shift keying would be the best encoding method to utilise, particularly in terms of signal robustness.

Results of harvesting acoustic signals to provide power for recharging *in vivo* biomedical devices are also presented. For the piezoelectric transducer used, we show the current-voltage, and voltage-power characteristic curves. These are compared with theoretical models of the power generation. Power requirements for pacemakers are discussed, and how acoustic power harvesting could be successfully used to recharge the devices over their respective lives.

2. Background

Biomedical devices implanted within the human body have been used since last century, starting with the cardiac pacemaker. Cardiac pacemakers are a ubiquitous technology, with over 3 million implanted worldwide (Wood & Ellenbogen, 2002). Since then, *in vivo* biomedical devices have been utilised for further applications. The "pacemaker", a term now used as a general device that generates electrical pulses within the human body, has been applied to the regulation of a number of conditions beyond their primary application for cardiac arrhythmia. When used in the brain, the technique of alleviating the symptoms of neurological disorders with electrical signals is called deep brain stimulation. Although the use of direct brain stimulation began as early as 1947 (Hariz et al., 2010), the use of a permanent pacemaker for deep brain stimulation is a much more recent development (Varadan, 2007). These pacemakers for neurological conditions have been developed recently primarily as a result of improve surgical and imaging techniques associated with neurology (Elias & Lozano, 2010).

Elias and Lozano (2010), give an overview of the current applications of deep brain stimulation. Neurological pacemakers have been applied in the brain for movement disorders, including Parkinson's disease, tremors, and dystonia. Also, they have been used for the treatment of psychological problems such as depression and obsessive-compulsive disorder. Current research on the topic is investigating the use of neurological pacemakers for epilepsy, cluster headache, impaired consciousness, and morbid obesity. Pacemakers have also been used for pain management, particularly pain associated with severe back problems (Blain, 2009).

Currently, pacemakers have their batteries replaced after a five year period. Typically, the entire pacemaker is removed, leaving the electrodes implanted. The battery life of a cardiac pacemaker can be assessed using magnet electrocardiographic assessment. This can even be performed over the telephone using transtelephonic monitoring (Schoenfeld, 2009). For implantable cardioverter-defibrillators, radiofrequency transmissions are used in their assessment, which has proven more effective than transtelephonic monitoring (Crossley et al., 2009). However, the primary advantage of acoustic transmission is not only the ability to safely conduct device follow-up for history taking, physical examination, electrocardiography, radiography, interrogation, and reprogramming (Schoenfeld & Blitzer, 2008). Acoustic transmissions will allow for *in vivo* recharging of the battery, reducing the number of surgeries associated with pacemaker replacement, ideally down to zero, depending on the battery itself.

3. Theory

3.1 Piezoelectric transducer

For a complete understanding of piezoelectric materials and transducers, see Silk's Ultrasonic Transducers for Nondestructive Testing (1984). A brief overview is included here for completeness.

The term piezoelectric means electricity from pressure. So as a force, either in the form of a pressure or a stress (both measured in force per unit area), is applied to the transducer, an electric signal is generated. Specifically, a charge dipole is generated within the crystal structure of the material, which when used inside of a capacitor, results in the generation of a voltage drop across the transducer.

In linear elastic solids, the strain (S) and stress (T) are related by the elastic stiffness (c). In the same material, the electric displacement (D) is related to the electric field (E) by the permittivity (ε_r) of the material. These equations are referred to as the constitutive equations. In a piezoelectric linear elastic material, the constitutive equations are coupled. Hence, a change in stress or strain corresponds to a change in the charge distribution within the material. The constitutive equations for a piezoelectric material are,

$$\begin{aligned} T &= cS + hE \\ D &= \varepsilon_r E + hS, \end{aligned} \tag{1}$$

where h is the piezoelectric coupling coefficient.

Fig. 1(a) shows the crystal lattice structure of lead zirconate titanate (PZT), a peizoceramic material. As a force is applied to the crystal, the lattice is strained, and a charge dipole is produced, similar to that seen in Fig. 1(b).

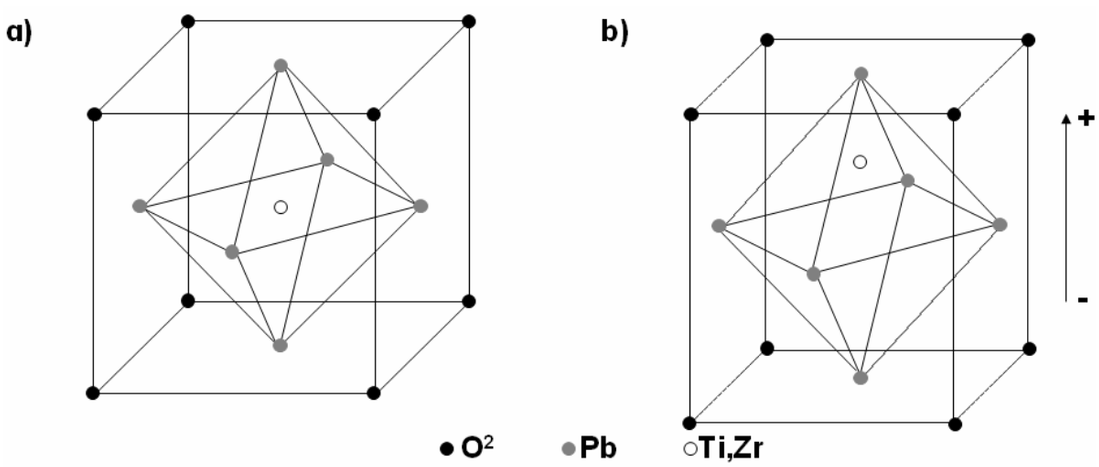

Fig. 1. Principle behind the use of a piezoelectric material, both before (a) and after (b) strain.

3.2 Digital communications

Due to the properties of the communications channel, only digital encoding methods have been investigated. The primary benefit of digital encoding is improved fidelity. The three basic digital encoding methods used include amplitude shift keying, frequency shift keying, and phase shift keying. For the purpose of concept demonstration, only binary keying methods were utilized.

3.2.1 Amplitude shift keying.

In amplitude shift keying, the digital information is encoded onto the analogue carrier as a time varying signal of the amplitude. The simplest form of amplitude shift keying is on-off keying, where a '1' is represented by the amplitude function being maximum (on), and a '0'

is represented by the amplitude function being zero (off). The on-off keying signal will have the form,

$$f(t) = A(t)\cos(2\pi f_c t), \tag{2}$$

where f_c is the carrier frequency, and,

$$A(t) = \begin{cases} 0 & for\ data = 0 \\ A & for\ data = 1. \end{cases} \tag{3}$$

On-off keying is decoded by using a rectifier and a low-pass filter that has a cut-off frequency above the data rate, but below the carrier frequency. This removes the carrier wave component ($\cos(2\pi f_c t)$) and recovers the amplitude function which is the digital signal ($A(t)$).
Fig. 2 shows the decoding process for an amplitude shift keying signal. Fig. 2 (a) shows the data to be transmitted defined by (3); Fig. 2 (b) shows the on-off keying signal defined by (2). The received signal is then rectified and low-pass filtered, to remove the carrier frequency, shown in Fig. 2 (c). This also results in some distortion of the information signal due to the removal of higher harmonics. Hence, the signal is passed through a comparator to recover the digital information as shown in Fig. 2 (d).

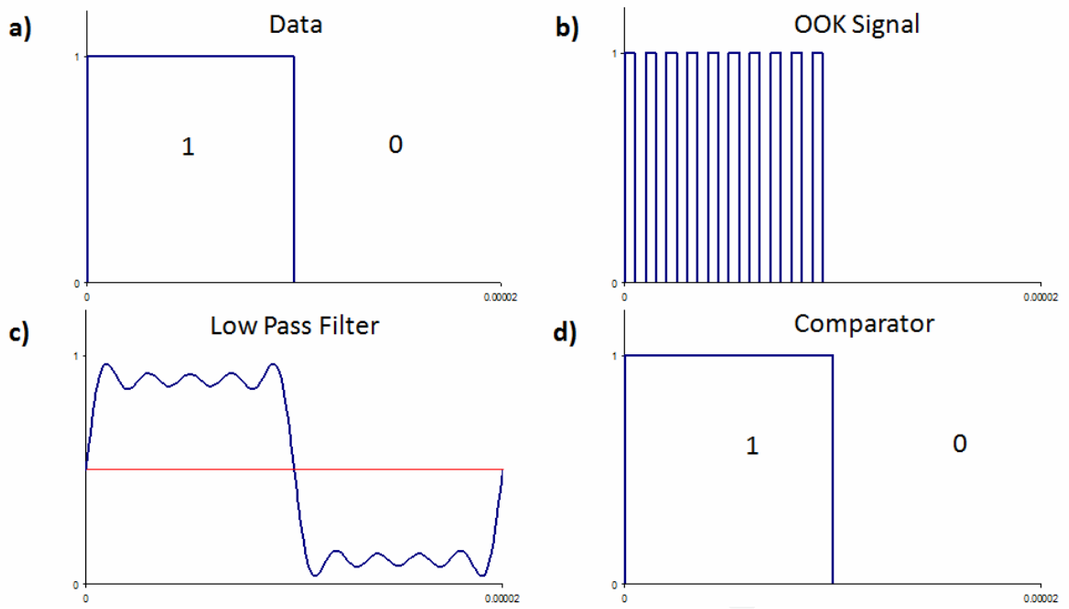

Fig. 2. Decoding an amplitude shift keying signal, a) the digital data to be transmitted, b) the on-off keying signal, c) the rectified low-pass filtered signal, d) digital information recovered after a comparator.

3.2.2 Frequency shift keying.

In frequency shift keying the digital information is encoded onto the analogue carrier as a time varying signal of the frequency. In binary frequency shift keying, two frequencies are used; one frequency represents a digital '1' and the second represents a digital '0'. Frequency shift keying can be thought of as two interweaved on-off keying signals with

different carrier frequencies. This means that a similar non-coherent decoding method can be used to recover the digital information. However, the advantage frequency shift keying has over amplitude shift keying is lost in this way. To maintain the independence of the signal from amplitude variations, a coherent detection method is used. Here, the received signal is split into two separate, but identical signals; each of the form,

$$f(t) = A_0 \cos\left(2\pi f_c(t)t\right), \tag{4}$$

where,

$$f_c(t) = \begin{cases} f_1 & for\ data = 0 \\ f_2 & for\ data = 1. \end{cases} \tag{5}$$

The two signals are each multiplied with a synchronous sinusoid, one with frequency f_1, the other with frequency f_2. This shifts the signal to zero and $2f_n$. A low pass filter is used to remove the $2f_n$ component from each signal. The two filtered signals are then compared to each other to recover the digital information.
In Fig. 3 we see the stages involved in the decoding of a frequency shift keying signal. The data transmitted, Fig. 3 (a), is encoded as two separate frequencies in the signal, defined by (4). The received signal is then split into two identical signals, each mixed with a sinusoid at one of the two frequencies, shown in Fig. 3 (c). Here one of the data bits has no offset, while the second bit has an offset. When filtered, the lack of an offset will result in a zero, while an offset will give a one. The recovered signal after the filter and comparator is shown in Fig. 3 (d).

3.2.3 Phase shift keying.

In phase shift keying, the digital information is encoded onto the analogue carrier as a time varying signal of the phase. Decoding phase shift keying uses some simple mathematics to retrieve the phase information. The phase shift keying signal,

$$f(t) = A_0 \cos\left(2\pi f_c t + \phi(t)\right), \tag{6}$$

where,

$$\phi(t) = \begin{cases} -90 & for\ data = 0 \\ 90 & for\ data = 1, \end{cases} \tag{7}$$

is multiplied by a synchronous sine and cosine, giving,

$$\begin{aligned} h(t) &= A_0 \cos(2\pi f_c t + \phi(t)) \times \sin(2\pi f_c t) \\ &= \frac{A_0}{2}[\sin\left(\left(4\pi f_c t + \phi(t)\right)\right) + \sin\left(\phi(t)\right)], \end{aligned} \tag{8}$$

and,

$$\begin{aligned} g(t) &= A_0 \cos(2\pi f_c t + \phi(t)) \times \cos(2\pi f_c t) \\ &= \frac{A_0}{2}[\cos\left(\phi\right) + \cos\left(\left(4\pi f_c t + \phi(t)\right)\right)]. \end{aligned} \tag{9}$$

These two components are called the in-phase (I) and quadrature (Q) components. Both the in-phase and quadrature components contain high and low frequency components, where the low frequency component is the sine or cosine of the time dependent phase. Using a low pass filter the high frequency components are removed, leaving only the phase component,

$$\begin{aligned} h'(t) &= \frac{A_0}{2}\sin\left(\phi(t)\right), \\ g'(t) &= \frac{A_0}{2}\cos\left(\phi(t)\right). \end{aligned} \tag{10}$$

Then by taking the arc-tangent of I on Q, the time dependent phase information is recovered,

$$\begin{aligned} y(t) &= \arctan\left(\frac{h'(t)}{g'(t)}\right) \\ &= \arctan\left(\frac{\sin(\phi(t))}{\cos(\phi(t))}\right) \\ &= \arctan\left(\tan(\phi(t))\right) \\ &= \phi(t). \end{aligned} \tag{11}$$

Fig. 4 shows the decoding process for a phase shift keying signal. The digital information, Fig. 4 (a), is encoded onto the carrier as a 180 degree phase shift, as shown in Fig. 4 (b). The resultant in-phase and quadrature components after the signal mixing are shown in Fig. 4 (c). When filtered, the mixed signals show that the in-phase component has a positive value for the first bit, then a negative value for the second bit, while the quadrature component has a value of zero. The arc-tanagent of this ratio will then recover the digital information.

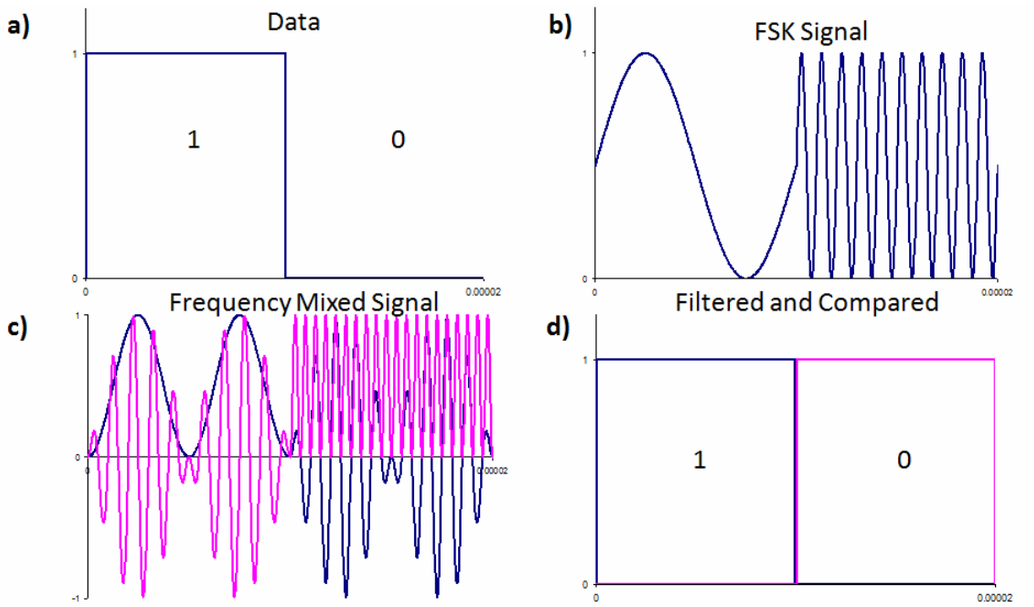

Fig. 3. Decoding a frequency shift keying signal, a) the digital data to be transmitted, b) the frequency shit keying signal, c) the frequency mixed signal, d) digital information recovered after filtering and comparing.

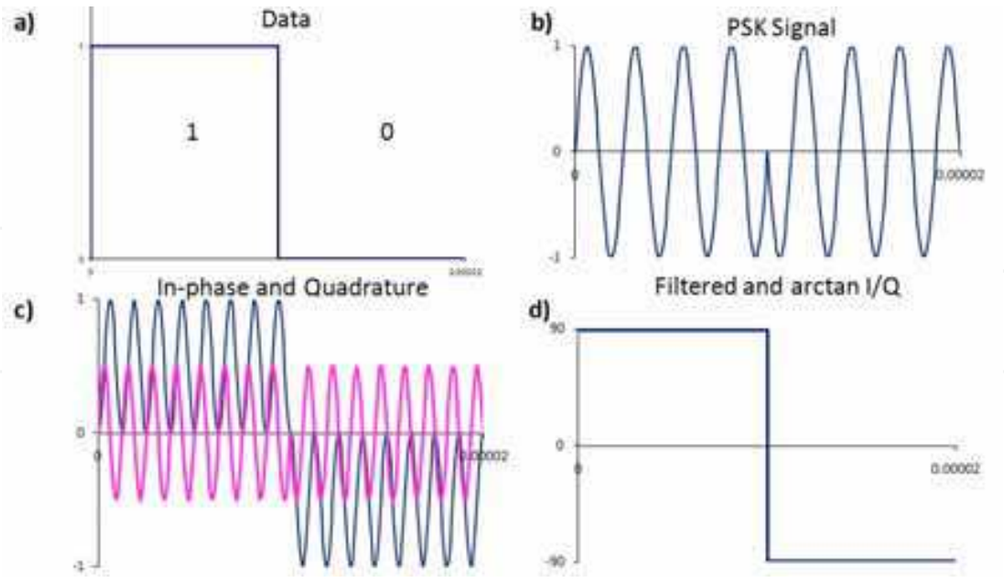

Fig. 4. Decoding a phase shift keying signal, a) the digital data to be transmitted, b) the phase shift keying signal, c) the in-phase and quadrature components, d) digital information recovered after filtering and taking the arc-tangent.

3.3 Power harvesting

For the power harvesting, the piezoelectric receiver is modelled as a current source, i_P, in parallel with a capacitor, C_P. The source current can be written as (Ottman, et al., 2002),

$$i_P(t) = I_P \sin(\omega t), \tag{12}$$

where I_P is the peak current, also referred to as the short circuit current, and ω is the angular frequency of the alternating current signal. The open circuit voltage, V_{OC}, can then be defined in terms of the short circuit current and the reactance of the capacitor (X_C) (Guan & Liao, 2004), that is,

$$V_{OC} = I_P X_C = \frac{I_P}{\omega C_P}. \tag{13}$$

To harvest power, the piezoelectric element needs to be connected across a load. In the case of the alternating current analysis, this is simply a load resistance. There is a 90 degree phase shift between the current flowing through the load resistor (R) and the current flowing through the capacitor. The total power can be expressed as the geometric sum of the power stored in the capacitor, and the power dissipated through the resistor. That is,

$$\begin{aligned} P_T &= \sqrt{P_R^2 + P_C^2} \\ &= \sqrt{I_R^2 R + I_C^2 X_C}. \end{aligned} \tag{14}$$

Since the circuit is an alternating current current divider, the short circuit current can be expressed as,

$$I_P = \sqrt{I_R^2 + I_C^2}. \tag{15}$$

The peak power will then occur when the current flow through the capacitor and the resistor is equal. That is, the load resistance is equal to the capacitor's reactance,

$$R = \frac{1}{\omega C}. \tag{16}$$

The resistor current at peak power is then,

$$I_R = \frac{I_P}{\sqrt{2}}. \tag{17}$$

The voltage at peak power is then,

$$V_{\max} = I_R X_C = \frac{I_P}{\sqrt{2}\omega C_P}. \tag{18}$$

We can also express the voltage out as a function of the resistance. From (15) we see that,

$$V = RI_P = R\sqrt{I_P^2 - I_C^2}, \tag{19}$$

The capacitor current is also a function of the voltage, so with a little algebra we see (Ottman, et al., 2002),

$$V = \frac{I_P R}{\sqrt{1 + \left(\omega C_p R\right)^2}}. \tag{20}$$

The power as a function of the load resistance can then be expressed as,

$$P = \frac{V^2}{R} = \frac{I_P^2 R}{1 + \left(\omega C_p R\right)^2}. \tag{21}$$

4. Method

4.1 Acoustic channel configuration

The acoustic transmissions channel is shown in Fig. 5. The setup consists of a PZT transducer as the transmitter, coupled to one side of the forearm using acoustic coupling gel, and a second transducer on the opposite side as a receiver. The ultrasonic signals were generated by an arbitrary waveform generator, an Agilent 33120A. The received signals were recorded on a digital storage oscilloscope, an Agilent 54600A. The piezoelectric transducers used were Steiner and Martins SMQA PZTs, and were unbacked. They had a thickness of 2.1 millimetres, corresponding to a resonant frequency of 1 megahertz, and a radius of 10 millimetres.

4.2 Acoustic communications

Testing the communications involved looking at a number of different quantities. These included,

- the transfer function,
- the frequency response,

- the transient response,
- the digital encoding method, and,
- the data rate.

First, the transfer function of the communications channel was measured. The waveform generator was set to give a continuous sine wave at the resonant frequency of the PZT transducers, 1 megahertz. The amplitude was then varied from 1 volt to 10 volts. Values were recorded at 1 volt increments. This process was repeated several times to give an average and statistical uncertainty.

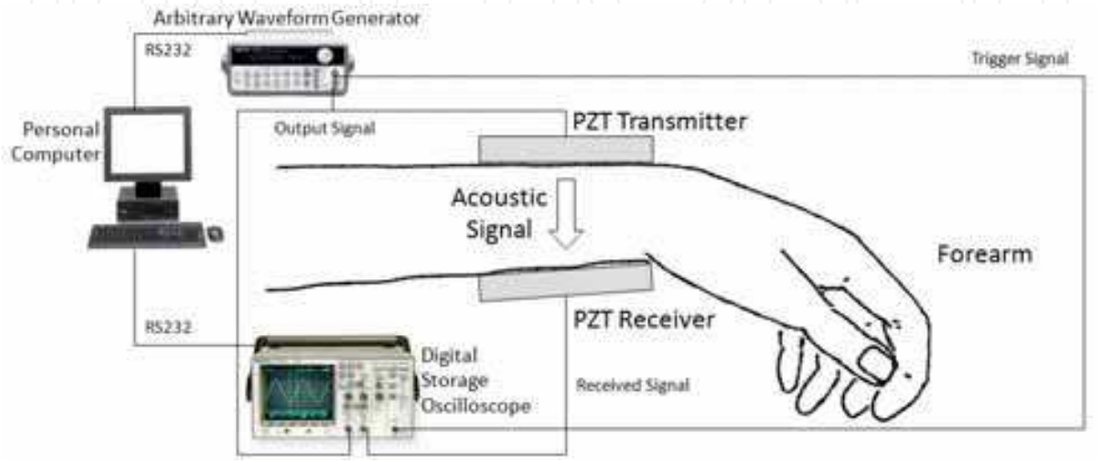

Fig. 5. The configuration of the acoustic transmissions channel through a forearm.

Next, the frequency responses of the communications channel were determined. The function generator was set to give a continuous sine wave at maximum voltage, 10 Volts peak. The frequency was then varied from 10 kilohertz to 1 megahertz. Values were recorded every 10 kilohertz.

Finally, the transient response of the communications channel was investigated, using a low rate sine wave burst at 1 megahertz with 100 cycles. The trailing signal was also examined to determine if it would have any adverse effects on the performance of the communications channel.

The communications signals were generated on the arbitrary waveform generator. Amplitude shift keying (specifically on-off keying) signals were generated using the burst function of the arbitrary waveform generator. A 1 megahertz sine wave carrier was used with a data rate of 40 kilobits per second. The waveform generator used had a built-in frequency shift keying function. This was used to generate the signals, with frequencies of 440 kilohertz and 880 kilohertz at a data rate of 14.5 kilobits per second. The phase shift keying signals were generated in the Waveform Editor software for the arbitrary waveform generator. The signals were then downloaded to the device via the computer interface. The generated waveform consisted of a sine wave carrier, with a data rate of 1/100 the carrier frequency (the software does not generate time so the frequency is set and varied on the generator, and hence a ratio is used for reference). Hence, for the carrier wave frequency of 1 megahertz, the data rate was 10 kilobits per second.

All of the communications signals were recorded on the digital oscilloscope, and downloaded to a personal computer. The demodulation of the signals was then implemented in Matlab™ (The Mathwork Inc). The filter used was a raised cosine filter (Proakis & Salehi, 1994).

4.3 Acoustic power transmission

For the preliminary acoustic power harvesting, the alternating current performance was analysed. In the alternating current circuit experiments, first the capacitance of the piezoelectric element was measured using a capacitance meter. After calculating the reactance at the resonant frequency, the output of the piezoelectric receiver was applied to a variety of suitable load resistors. The voltage drop across the load resistor was measured using a 1 megaohm digital storage oscilloscope. To compare the experimental results to the theoretical analysis, the alternating current circuit was also simulated in PSpice (Cadance Design Systems). The value of I_P was obtained using (13), with the measured values of C_P and V_{OC}. A parametric analysis was performed, varying the value of the load resistance in a frequency domain analysis. The load value was swept from 10 ohms to the value of the digital storage oscilloscope, 1 megaohm, at 10 points per decade. For the practical experiments, a decade resistance box was included, in parallel with the digital storage oscilloscope, as the load resistor. Fig. 6 shows the modified experimental setup for the acoustic power harvesting, and the circuit used in the simulations.

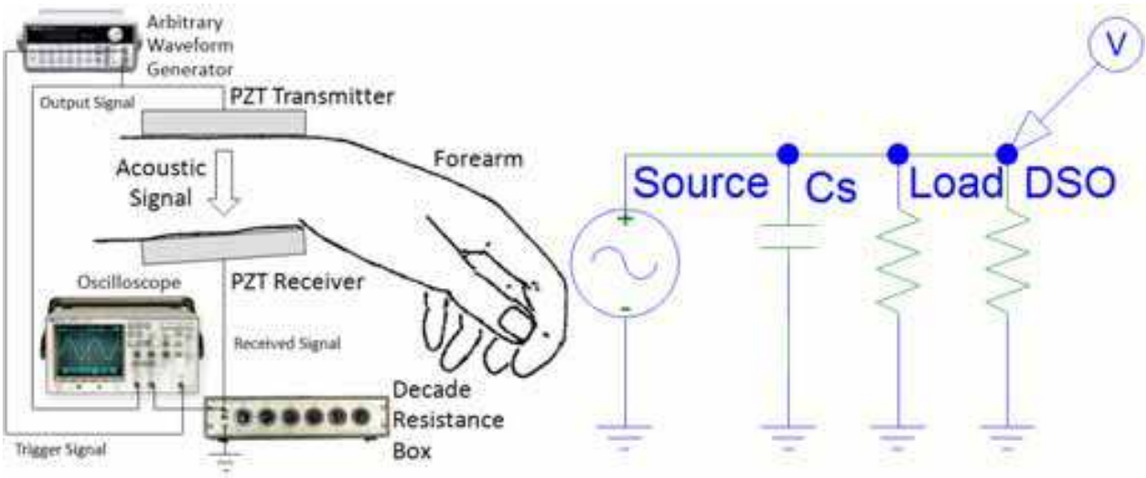

Fig. 6. The modified experimental setup for the acoustic power harvesting, shown left, and the circuit used in the simulation of the power harvesting, shown right.

5. Results

5.1 Transfer function

Fig. 7 shows the transfer function of the acoustic-communications channel at 1 megahertz. The relationship between the input signal strength and the output signal strength is linear, with a correlation coefficient of 1. The noise (and hence, error bars) in the curve is due to small movements in the transmission medium.

5.2 Frequency response

The frequency response of the acoustic-communications channel is shown in Fig. 8. As expected, a strong peak in the frequency spectrum occurs at the resonant frequency of the piezoelectric transducers, that is, 1 megahertz. A secondary peak is noticeable at 100 kilohertz.

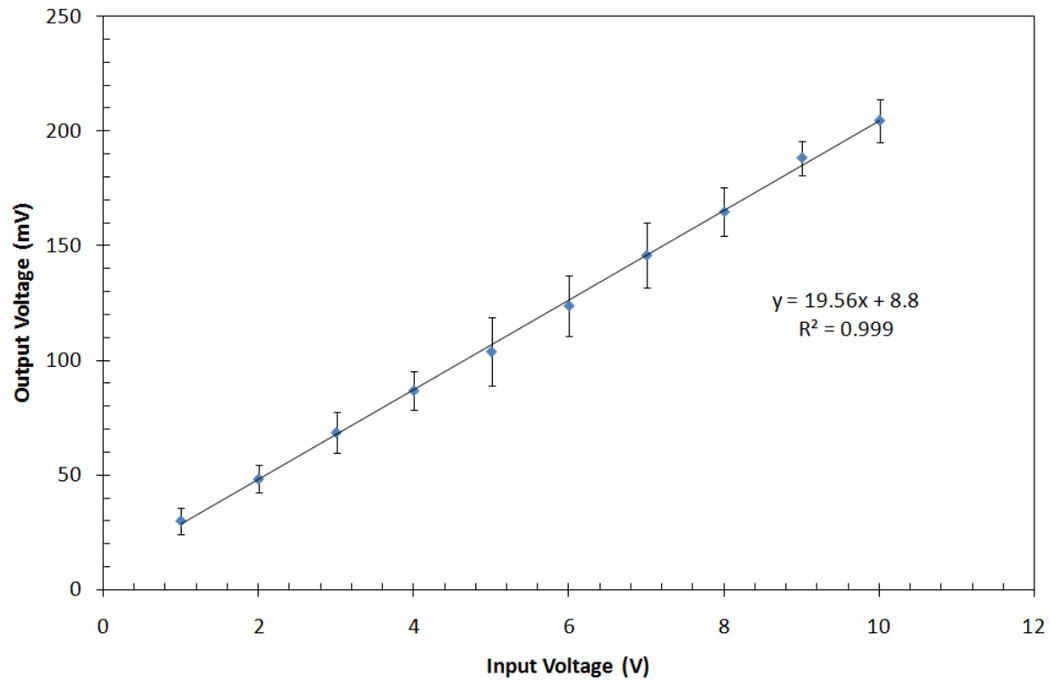

Fig. 7. The transfer function of the acoustic transmissions channel at resonance.

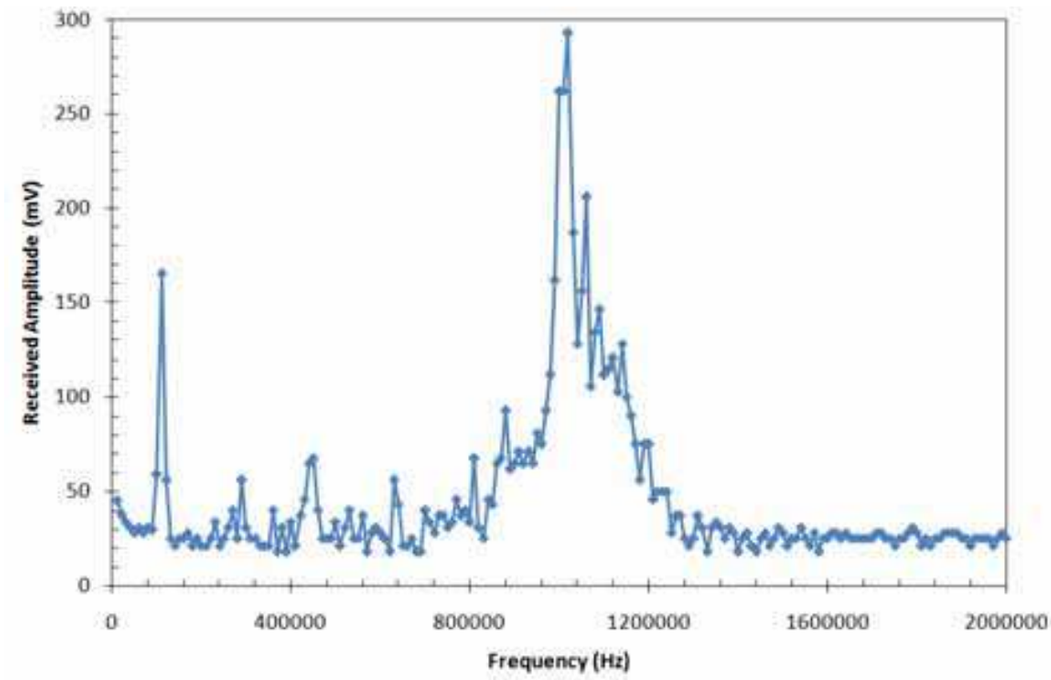

Fig. 8. The frequency response of the acoustic transmissions channel.

5.3 Transient response

Fig. 9 shows the transient response of the acoustic-communications channel for several cycles at 1 megahertz. The received tone burst is relatively compact, with a short transient

period, and only a small amount of signal in the tail. Fig. 10 shows the transient response with enough cycles to achieve steady-state. The rise time is then given by approximately 25 cycles, at 1 megahertz, giving 25 microseconds.

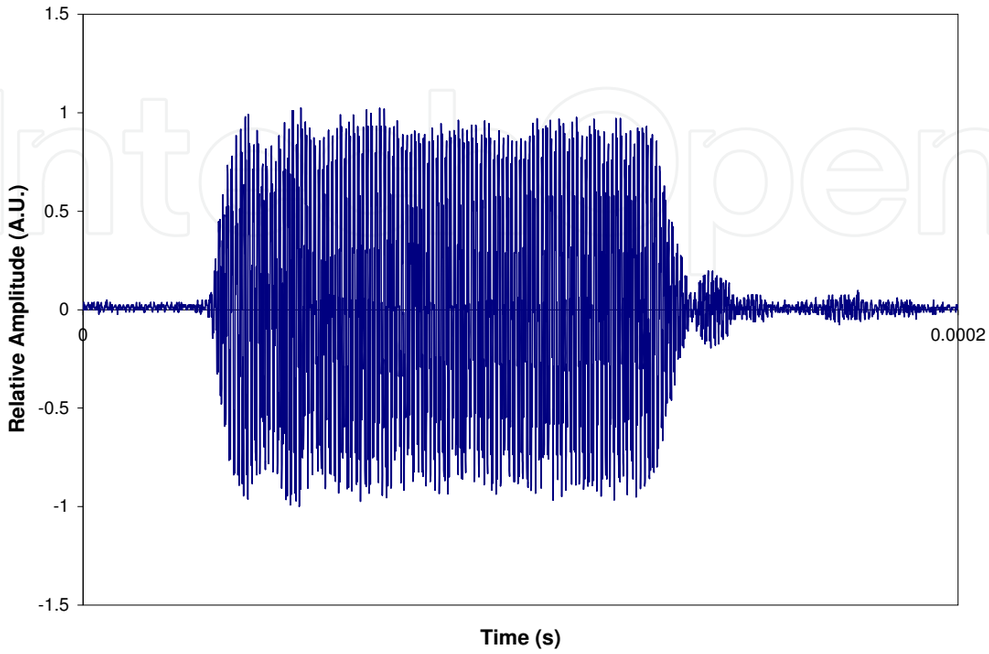

Fig. 9. The transient response of the acoustic transmissions channel at resonance with maximum amplitude, showing the full 100 cycle tone burst.

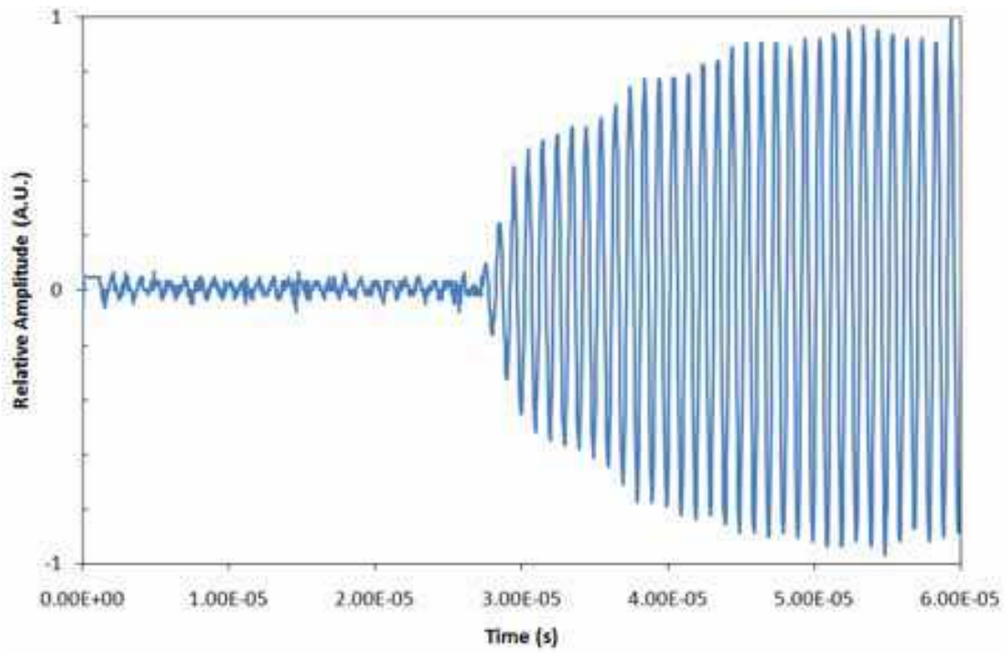

Fig. 10. The transient response of the acoustic transmissions channel at resonance with maximum amplitude, showing the number of cycles required to achieve steady state.

5.4 Communications signals

Fig. 11 shows the transmitted amplitude shift keying signal. Ringing is noticeable as the signal is switched off. Fig. 12 shows the received amplitude shift keying signal. A rectifier and a low pass filter above the data rate, but below the carrier frequency, will recover the envelope, and the use of a comparator with a suitable compare level will enable the digital information to be recovered. This step is not shown, as it simply recovers the four bits that corresponds exactly to the transmitted information.

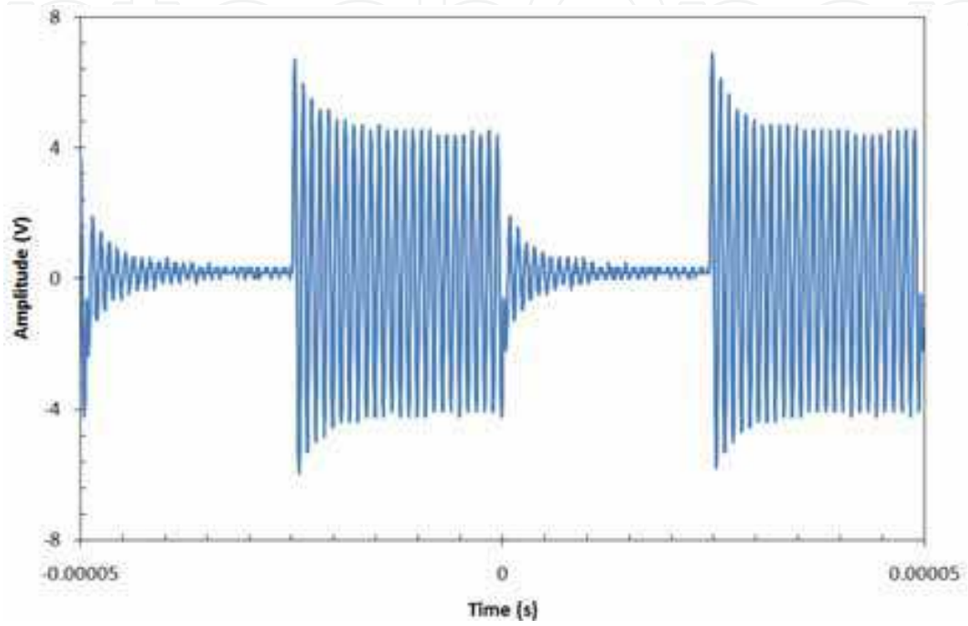

Fig. 11. The transmitted amplitude shift keying/on-off keying signal.

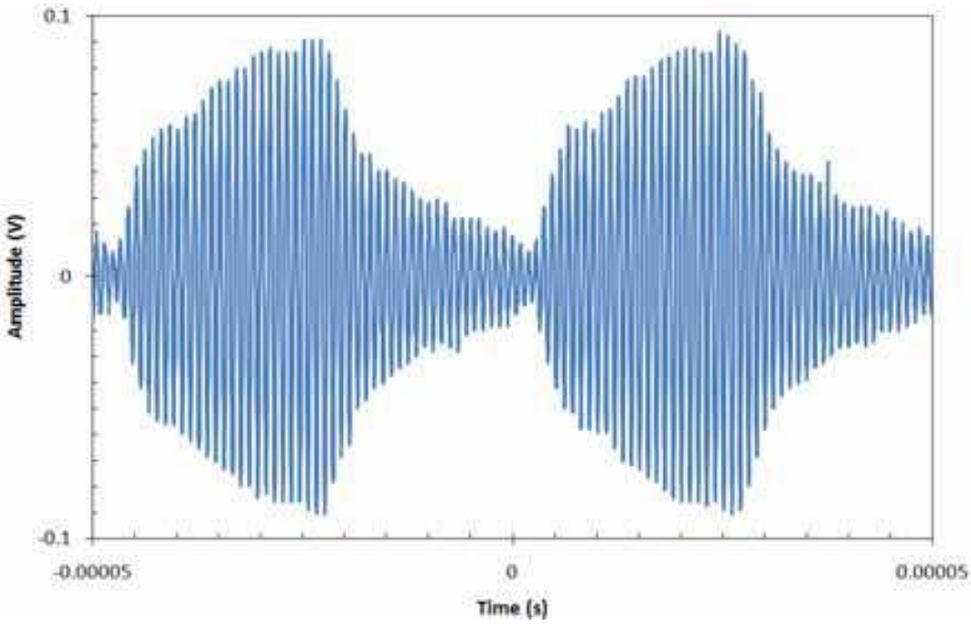

Fig. 12. The received amplitude shift keying/on-off keying communications signal.

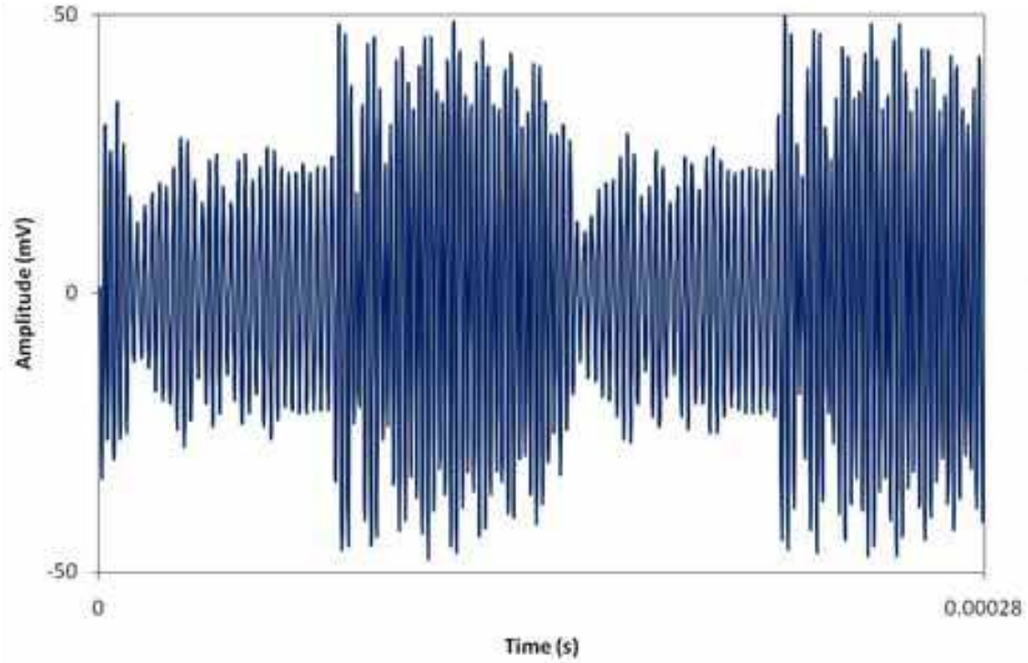

Fig. 13. The received frequency shift keying signal, showing the two frequency signals mixed together.

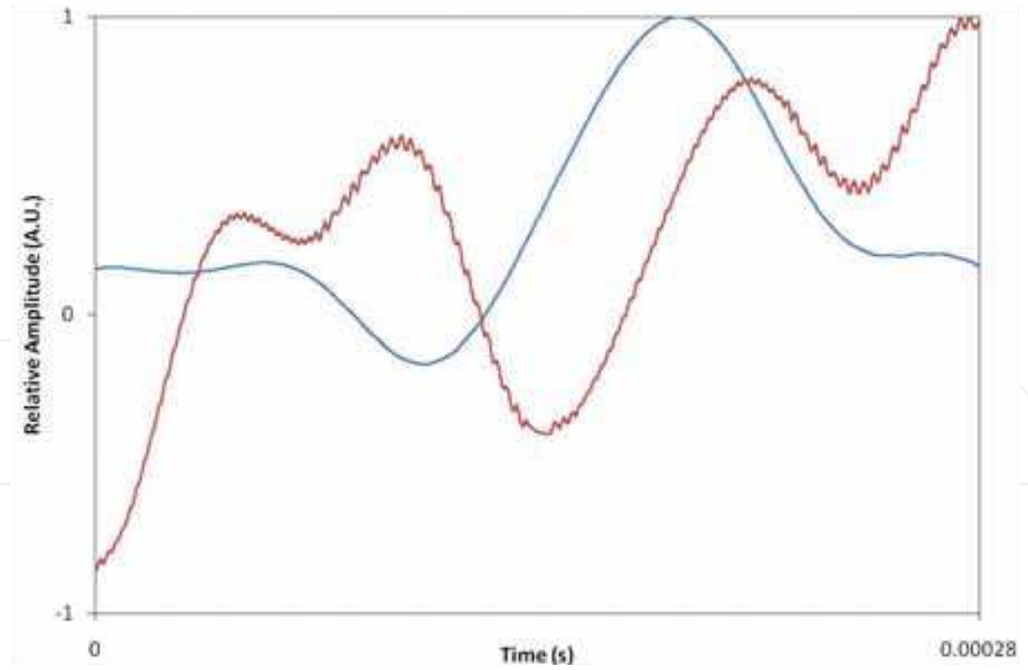

Fig. 14. The received frequency shift keying signal after signal mixing and filtering.

Fig. 13 shows the received frequency shift keying signal. A clear difference between the two frequency components can be seen. As expected, the 880 kilohertz signal has a larger amplitude, as a result of the improved channel response over the 440 kilohertz. Fig. 14 shows the signals after the frequency mixing and filtering. From here, there are four separate sections.

The first starts with the 880 kilohertz signal on top. From here, the signals cross over as expected, enabling the original digital information to be recovered by comparing the two signals to each other. An interesting point occurs around a quarter of the way in, where the two components nearly cross over again, which could result in a bit error. Hence, it is safe to assume that the data rate is almost at a maximum with frequency shift keying.

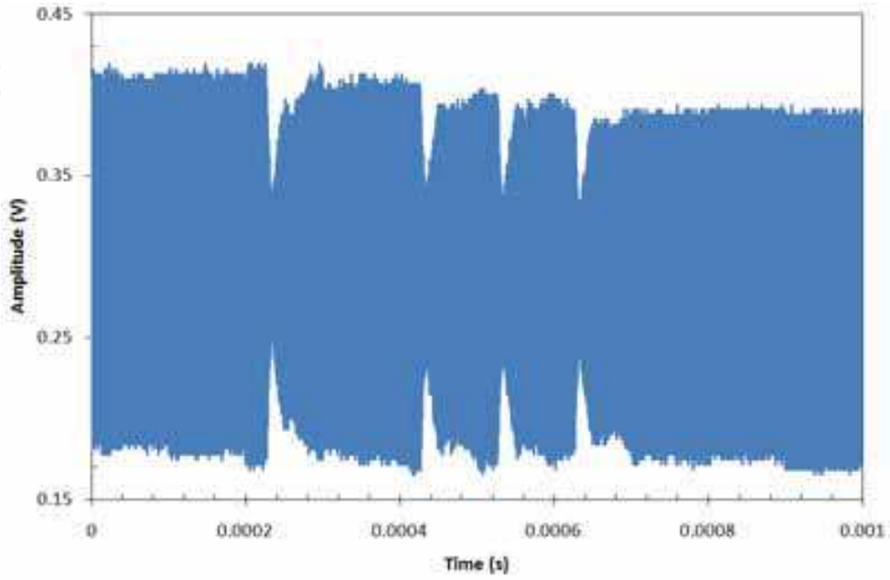

Fig. 15. The received phase shift keying signal, where the change in phase appears as a transient signal similar to the on-off keying of the signal.

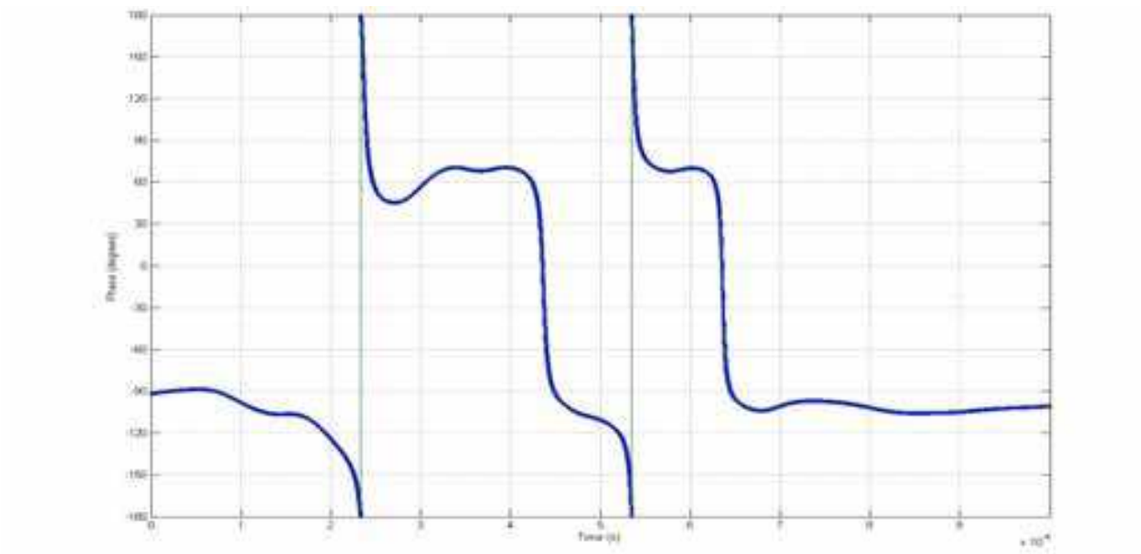

Fig. 16. The recovered phase information decoded from the received phase shift keying communications signal.

Fig. 15 shows the received phase shift keying signal, which contains the data stream [1 1 0 0 1 0 1 1 1 1]. The decoded phase shift keying signal is then shown in Fig. 16. The original

digital information can be recovered by selecting a digital 1 as a phase less than 0 degrees, and a digital 0 as a phase greater than 0 degrees. Note that the transmitted phase shift keying signal is not shown, as no information is visible on the time scale of the entire signal.

5.5 Power transmission

The capacitance of the piezoelectric receiver was measured to be 1.086 nanofrads. At the resonant frequency of 1.035 megahertz, this gives a reactance of 141 ohms. With an open circuit voltage of 570 millivolts, (13) gives a short circuit current of 4 milliamps. These values where then used in the PSpice simulation of the alternating current circuit.

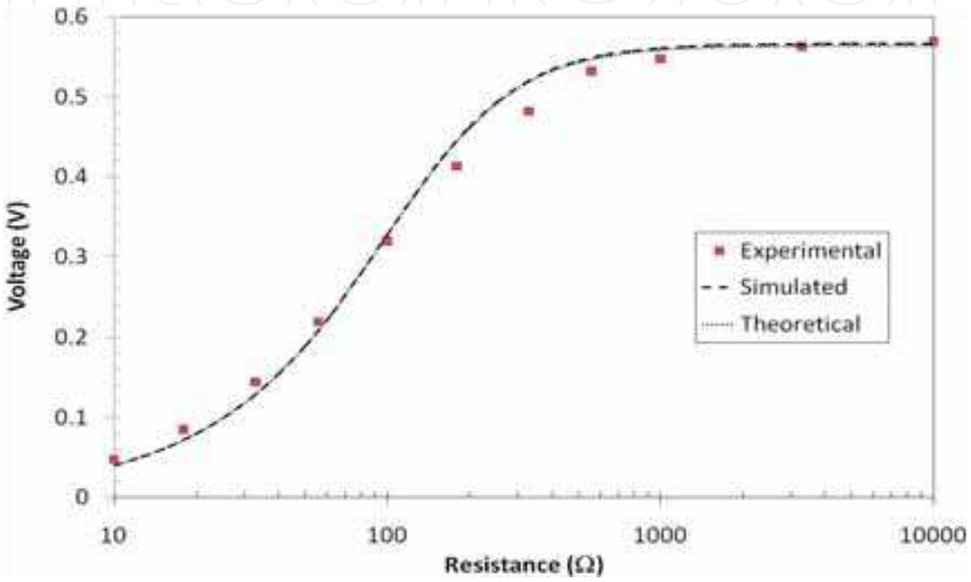

Fig. 17. Voltage as a function of load resistance for the power harvesting.

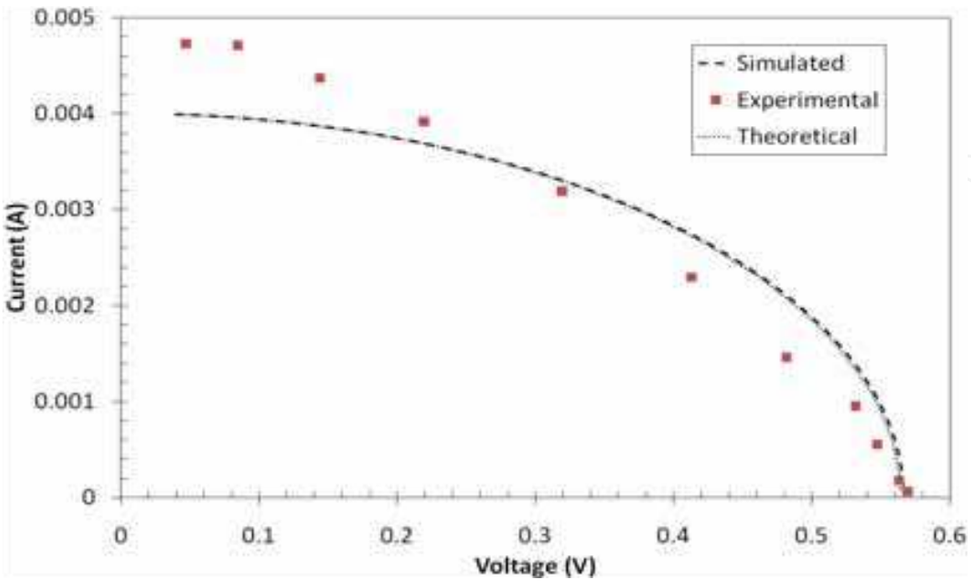

Fig. 18. Load current as a function of the voltage, current-voltage curves.

Fig. 17 shows the comparison between the applied load and the voltage drop across it, for both the experimental values and the simulated results. As expected, as the load resistance decreases in size, the output voltage also decreases.
Fig. 18 shows the load current as a function of the output voltage (current-voltage curves), and Fig. 19 shows the power delivered to the load as a function of the output voltage (power-voltage curves), for the experimental, theoretical and simulated results. The power-voltage curves shows a measured peak power of 1 milliwatt, while theory and simulation give peak power values of 1.121 milliwatts and 1.125 milliwatts, respectively.

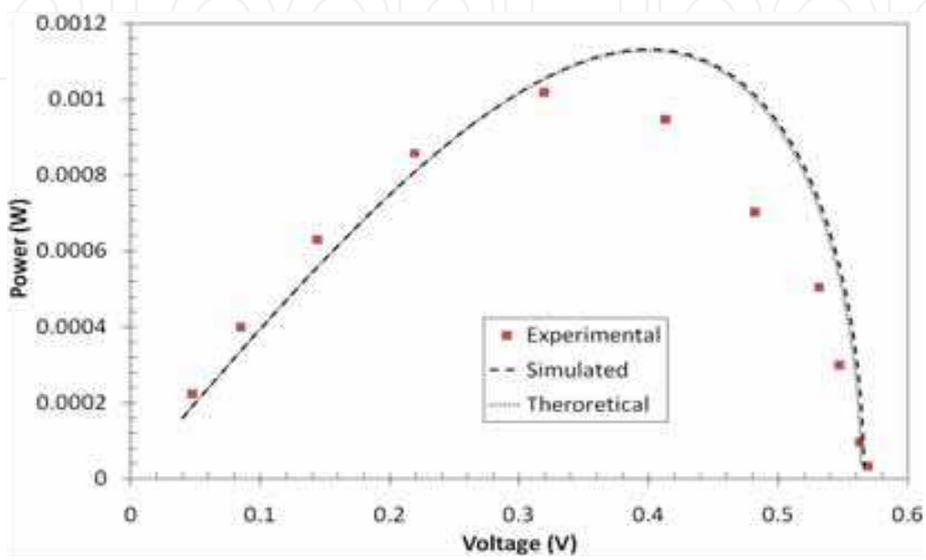

Fig. 19. Power delivered to the load as a function of the voltage, power-voltage curves.

6. Discussion

Another important advantage of acoustic communications is security. With implantable cardioverter-defibrillators utilising wireless radiofrequency communications, the security of the signal needs to be considered. A commercially avilable implantable cardioverter-defibrillator was easily attacked in a recent study (Halperin, et al., 2008). As a contact wireless communications method, acoustic transmissions are inherently secure, in that someone needs to touch you to be able to communicate with the *in vivo* biomedical device. From here, an encryption method could be utilised for communications if necessary. Halperin et al. suggest that encryption is expensive in the power budget. However, the use of acoustic power harvesting means that the power required for encryption would not be an issue.

6.1 Transmissions channel

As expected, the transfer function is linear. Some randomness is noticeable in the signal, hence the uncertainty. It is worth noting that a similar uncertainty would be expected on all other results. The experiments were performed with the arm as immobile as possible. A significant variation was noticed when the arm/hand was allowed to articulate. When deliberately trying to alter the output voltage, the peak value varied from around 140 millivolts to 280 millivolts, a factor of 2. This fluctuation may be an issue, in particular if amplitude shift keying is used as the encoding method. This is one of the reasons that phase shift keying would be a more robust encoding method for the communications signals.

The frequency response shows a strong primary resonance at the through thickness resonance of the transducer, 1 megahertz, and a secondary resonance at 100 kilohertz, corresponding to the radial resonance of the transducer. Overall, the frequency response of the transmissions channel suggests that frequency shift keying would not be suitable. However, there is a small resonance at 440 kilohertz, and another tertiary resonance at 880 kilohertz. Hence, these two frequencies were ideal to test frequency shift keying.
The transient response of the transmission channel is relatively neat. The compact form of the tone burst only has a minor tail effect, elongating the signal in time. One of the main reasons for this is due to the composite nature of the communications channel. The various materials which the body is made up of all have different acoustic velocities. The result of this is that the various paths travelled by the ultrasound in the medium will result in significant temporal dispersion, and then interference.

6.2 Acoustic communications

The result of the amplitude shift keying communications signal tests suggests that relatively high data rates could be achieved for the sort of information that needs to be transmitted. The amplitude shift keying signal is limited primarily by the transient response of the transmissions channel. That is, with a transient response time of 25 micro seconds, a data rate of 40 kilobits per second is possible when using a 1 megahertz carrier frequency. By utilising a transducer with a high resonant frequency, and a larger bandwidth, the achievable data rate could be significantly increased. However, amplitude shift keying has a limited effectiveness, particularly as the coupling efficiency varies with movement of the transmission medium (the forearm).
The frequency shift keying results suggest that the data rate may not be able to be improved much further. This is illustrated by the relative closeness of the two mixed signals in Fig. 14, approximately a quarter of the way through. The most likely cause of this is the frequency response. Since the 880 kilohertz signal is close to the resonant frequency of 1 megahertz, this could lead to a stronger amplitude in the 880 kilohertz signal, which is seen as the consistently higher signal strength of the corresponding mixed and filtered signal (Fig. 14, red trace). The resultant “steady state” frequency will also be affected by the resonant frequency of the transducer, which will be given as a combination of the driving frequency, and the resonant frequency. This explains the drift shown in Fig. 14, where the curves both steadily increase.
The recovered phase information, from the phase shift keying signal, suggests that a relatively high data rate is possible. The phase transitions indicate that a data rate up to that of the amplitude shift keying signal (40 kilobits per second) could be used. However, unlike the amplitude shift keying signal, the phase shift keying has robustness relative to the amplitude variation in the received signal. The phase transitions are not as quick as those shown in previous work (Wild & Hinckley, 2010), when communicating through an aluminium panel, but as previously mentioned, the data rate is relatively high for the intended application. The primary advantage of a high communications rate would be to reduce the effect of fluctuations due to motion of the communications medium.

6.3 Power harvesting

The preliminary results for the power harvesting are promising. The value of 1 milliwatt was significant compared to values expected. However, in the attempt to implement an alternating-current to direct-current converter circuit, the very high frequency (1 megahertz) appears to be limiting the ability to successfully rectify the output of the transducer. This is

mainly due to the high junction capacitance of the rectifier diodes. In the conversion from alternating-current to direct-current, the capacitance is an important consideration to achieve peak power output (Ottman et al., 2002). To resolve this issue, transducers with a lower resonant frequency, in the kilohertz range, need to be utilised. Ideally, broadband transducers could be used to quantify the performance of the power conversion as a function of frequency, as (13) indicates that the higher the frequency, the less power that can be generated. In addition to this, the overall output voltage needs to be a larger amplitude. This is required due to the loss associated with the use of the diode rectifier circuit to convert the alternating-current to direct-current, which is required to power the actual biomedical device. This could be achieved in two ways; according to the transfer function the input voltage could be increased. However, it would be more effective if the efficiency of the channel could be improved. This could be achieved by selecting a transducer with a resonant frequency equal to the resonant frequency of the channel, which is related to the thickness of the channel, and the acoustic velocity.

Overcoming the two limitations encountered here with these preliminary results, could yield relatively large power generation. That is, with the successful implementation of an alternating-current to direct-current converter circuit, using a lower frequency, and a more efficient transfer of acoustic energy through the channel, the measured power levels could easily be utilised for the *in vivo* recharging of a device such as a pacemaker, which have relatively lower power consumptions (Mallela et al., 2004).

7. Conclusion

Successful communication was achieved through the communications channel. We also show the result of harvesting acoustic signals to provide power for recharging *in vivo* biomedical devices. In future work, we will optimise the transducers used to maximise the amplitude of the received acoustic transmissions. This is primarily a concern for the acoustic power harvesting, which will also include the implementation of adaptive direct current to direct current power converters to track the peak power point, to ensure efficient power transfer.

8. References

Blain, L. (2009). Spinal Cord Stimulators - the 'pacemaker' for chronic pain, *Gizmag*, (12 August 2009), viewed 8 September 2010, < http://www.gizmag.com/eon-mini-spinal-cord-stimulator/12486/>

Crossley, G.H., Chen, J., Choucair, W., Cohen, T.J., Gohn, D.C., Johnson, W.B., Kennedy,E.E., Mongeon, L.R., Serwer, G.A., Qiao, H. & Wilkoff, B.L. (2009). Clinical Benefits of Remote Versus Transtelephonic Monitoring of Implanted Pacemakers, *Journal of the American College of Cardiology*, Vol. 54, No. 22, (November 2009) 2012–2019, ISSN 0735-1097

Elias, W.J. & Lozano, A.M. (2010). Deep brain stimulation: the spectrum of application, *Neurosurgical Focus*, Vol. 29, No. 2, (August 2010) Introduction, ISSN 1092-0684

Gabriel, C., Gabriely, S. & Corthout, E. (1996a). The dielectric properties of biological tissues: I. Literature survey, *Physics in Medicine and Biology*, Vol. 41, No. 11, (November 1996) 2231–2249, ISSN 1361-6560

Gabriely, S., Lau, R. W. & Gabriel, C. (1996b). The dielectric properties of biological tissues: II. Measurements in the frequency range 10 Hz to 20 GHz," *Physics in Medicine and Biology*, Vol. 41, No. 11, (November 1996) 2251–2269, ISSN 1361-6560

Gabriely, S., Lau, R. W. & Gabriel, C. (1996c). The dielectric properties of biological tissues: III. Parametric models for the dielectric spectrum of tissues," *Physics in Medicine and Biology*, Vol. 41, No. 11, (November 1996) 2271–2293, ISSN 1361-6560

Guan, M. & Liao, W.H. (2005). Comparative analysis of pie-zoelectric power harvesting circuits for rechargeable batteries, *Proceedings of the 2005 IEEE International Conference on Information Acquisition*, pp. 243-246, ISBN 0-7803-9303-1, Hong Kong and Macau China, June 2005, IEEE Press, Washington DC

Halperin, D., Heydt-Benjamin, T.S., Ransford, B., Clark, S.S., Defend, B., Morgan, W., Fu, K., & Kohno, T., (2008). Pacemakers and Implantable Cardiac Defibrillators: Software Radio Attacks and Zero-Power Defenses, *Proceedings of the 2008 IEEE Symposium on Security and Privacy*, pp. 129-142, ISBN 978-0-7695-3168-7, Oakland, Ca, May 2008, IEEE Press, Washington DC

Hariz, M.I., Blomstedt, P. & Zrinzo, L. (2010). Deep brain stimulation between 1947 and 1987: the untold story, *Neurosurgical Focus*, Vol. 29, No. 2, (August 2010) E1, ISSN 1092-0684

Kim, C., Lehmanna, T. & Nooshabadib, S. (2007). An Ultra-Wideband Transceiver for Biotelemetry Systems, *Proceedings of SPIE Microelectronics: Design, Technology, and Packaging III*, ISBN 9780819469694, Canberra, December 2007, SPIE, Bellingham

Mallela, V.S., Ilankumaran, V. & Rao, N.S. (2004). Trends in cardiac pacemaker batteries, *Indian Pacing Electrophysiology Journal*, Vol. 4, No. 4, (October 2004) 201–212, ISSN 0972-6292

Ottman, G.K., Hofmann, H.F., Bhatt, A.C. & Lesieutre, G.A. (2002). Adaptive piezoelectric energy harvesting circuit for wireless remote power supply, *IEEE Transactions on Power Electronics*, Vol. 17, No. 5, (September 2002) 669-676, ISSN 0885-8993

Proakis, J., Salehi, M. (1994). *Communication Systems Engineering*, Prentice Hall, ISBN 978-0131589322, New Jersey, USA,

Schoenfeld, M.H. (2009). Transtelephonic Versus Remote Monitoring of Cardiovascular Implantable Electronic Devices, *Journal of the American College of Cardiology*, Vol. 54, No. 22, (November 2009) 2020–2022, ISSN 0735-1097

Schoenfeld, M.H., & Blitzer, M,L. (2008). Follow-up assessments of the pacemaker patient, In: *Cardiac Pacing and ICDs, 5th edition*, Ellenbogen K.A. & Wood M.A. (Eds.), 498 – 545, Wiley-Blackwell, ISBN 978-1-4051-6350-7, Hoboken, NJ

Silk, M.G. (1984). *Ultrasonic Transducers for Nondestructive Testing*, Adam Hilger Ltd, ISBN 0852744366, Bristol, UK.

Varadan, V.K. (2007). The role of Nanotechnology and Nano and Micro-Electronics in monitoring and control of Cardiovascular Diseases and Neurological Disorders, *Proceedings of SPIE Nanosensors, Microsensors, and Biosensors and Systems 2007*, ISBN 9780819466495, San Diego, March 2007, SPIE, Bellingham

Wild, G. & Hinckley, S. (2010). PSpice Simulation of an Electro-Acoustic Communications Channel, *IEEE Transactions on Ultrasonics, Ferroelectrics and Frequency Control*, Vol. 57, No. 4, (April 2010) 981-985, ISSN 0885-3010

Wood, M.A. & Ellenbogen, K.A. (2002). Cardiac Pacemakers From the Patient's Perspective, Circulation, Vol. 105, No. 18, (May 2002) 2136-2138, ISSN 1524-4539

Biomedical Engineering, Trends in Electronics, Communications and Software

Edited by Mr Anthony Laskovski

ISBN 978-953-307-475-7
Hard cover, 736 pages
Publisher InTech
Published online 08, January, 2011
Published in print edition January, 2011

Rapid technological developments in the last century have brought the field of biomedical engineering into a totally new realm. Breakthroughs in materials science, imaging, electronics and, more recently, the information age have improved our understanding of the human body. As a result, the field of biomedical engineering is thriving, with innovations that aim to improve the quality and reduce the cost of medical care. This book is the first in a series of three that will present recent trends in biomedical engineering, with a particular focus on applications in electronics and communications. More specifically: wireless monitoring, sensors, medical imaging and the management of medical information are covered, among other subjects.

How to reference

In order to correctly reference this scholarly work, feel free to copy and paste the following:

Graham Wild and Steven Hinckley (2011). Wireless Communications and Power Supply for In Vivo Biomedical Devices Using Acoustic Transmissions, Biomedical Engineering, Trends in Electronics, Communications and Software, Mr Anthony Laskovski (Ed.), ISBN: 978-953-307-475-7, InTech, Available from: http://www.intechopen.com/books/biomedical-engineering-trends-in-electronics-communications-and-software/wireless-communications-and-power-supply-for-in-vivo-biomedical-devices-using-acoustic-transmissions

INTECH
open science | open minds

InTech Europe
University Campus STeP Ri
Slavka Krautzeka 83/A
51000 Rijeka, Croatia
Phone: +385 (51) 770 447
Fax: +385 (51) 686 166
www.intechopen.com

InTech China
Unit 405, Office Block, Hotel Equatorial Shanghai
No.65, Yan An Road (West), Shanghai, 200040, China
中国上海市延安西路65号上海国际贵都大饭店办公楼405单元
Phone: +86-21-62489820
Fax: +86-21-62489821

IntechOpen